

CNN aided Weighted Interpolation for Channel Estimation in Vehicular Communications

Abdul Karim Gizzini, Marwa Chafii, Ahmad Nimr, Raed M. Shubair, *Senior Member, IEEE*, and Gerhard Fettweis, *Fellow, IEEE*

Abstract—IEEE 802.11p standard defines wireless technology protocols that enable vehicular transportation and manage traffic efficiency. A major challenge in the development of this technology is ensuring communication reliability in highly dynamic vehicular environments, where the wireless communication channels are doubly selective, thus making channel estimation and tracking a relevant problem to investigate. In this paper, a novel deep learning (DL)-based weighted interpolation estimator is proposed to accurately estimate vehicular channels especially in high mobility scenarios. The proposed estimator is based on modifying the pilot allocation of the IEEE 802.11p standard so that more transmission data rates are achieved. Extensive numerical experiments demonstrate that the developed estimator significantly outperforms the recently proposed DL-based frame-by-frame estimators in different vehicular scenarios, while substantially reducing the overall computational complexity.

Index Terms—Channel estimation, deep learning, IEEE 802.11p standard, vehicular communications.

I. INTRODUCTION

In practical vehicular applications, the communication reliability between vehicles is very important. In general, communication reliability can be evaluated by the accurate data recovery of the transmitted data at the receiver which depends primarily on the channel estimation accuracy. A precisely-estimated channel is critical for the equalization, demodulation, and decoding operations to follow. Hence, an accurate and robust channel estimation is essential for improving the overall system performance. Accurate channel estimation in vehicular communication is a challenging task, since in vehicular environments wireless channels have a high Doppler shift and a large delay spread [1]. As a result, the channel shows time and frequency selective fading characteristics due to motion and multi-path components. This double selectivity arises in high mobility vehicular environment where the channel rapidly varies within the transmitted frame.

IEEE 802.11p frame structure [2] allocates two full preamble symbols that are used for basic least square (LS) estima-

tion, and four pilot subcarriers within the transmitted data symbols which are used for channel variation tracking over time. This basic estimation at the beginning of the frame is simple, but it becomes invalid for the equalization of the successive transmitted symbols as a result of high channel variation in vehicular environments. Several conventional symbol-by-symbol (SBS) estimators have been proposed in the literature to improve the basic LS estimation performance [3]–[5].

Recently, deep learning (DL) algorithms have been integrated into wireless communications physical layer applications [6], [7] including channel estimation [8]–[10], due to its great success in improving the overall system performance, especially when employed on top of low-complexity conventional estimators. DL algorithms are characterized by robustness, low-complexity, and good generalization ability making the integration of DL into communication systems beneficial. Motivated by these advantages, DL algorithms have been used in IEEE 802.11p channel estimators in two different manners: (i) Feed-forward deep neural networks with different architectures and configurations are employed on top of SBS estimators [11]–[13], where the channel is estimated for each received data symbol directly. (ii) Convolutional neural networks (CNNs) are integrated in the frame-by-frame (FBF) estimators, where the estimated channel for the whole frame is considered as a 2D low resolution noisy image and CNN-based processing is applied as super resolution and denoising techniques. The higher performance accuracy can be achieved by employing FBF estimators, since the channel estimation of each symbol takes advantage from the knowledge of previous, current, and future allocated pilots within the frame. Unlike, SBS estimators, where only the previous and current pilots are employed in the channel estimation for each received symbol. In this paper, we will focus on FBF estimators, especially, the recently proposed CNN-based ones.

In [14], the authors propose CNN-based channel estimator denoted as channel network (ChannelNet), that employs radial basis function (RBF) interpolation as an initial channel estimation, after that the RBF estimated channel is considered as a low resolution image, where super resolution CNN (SR-CNN) followed by denoising CNN (DN-CNN) are integrated on top of the RBF estimated channel.

ChannelNet estimator suffers mainly from high computational complexity and considerable performance degradation in high mobility vehicular scenarios. Temporal spectral ChannelNet (TS-ChannelNet) has been proposed in [15], where average decision-directed with time truncation (ADD-TT) interpolation that is based on the demodulation and averaging

Authors acknowledge the CY Initiative of Excellence for the support of the project through the ASIA Chair of Excellence Grant (PIA/ANR-16-IDEX-0008).

Abdul Karim Gizzini, and Marwa Chafii are with ETIS, UMR8051, CY Cergy Paris Université, ENSEA, CNRS, France (e-mail: {abdulkarim.gizzini, marwa.chafii}@ensea.fr).

Ahmad Nimr, and Gerhard Fettweis are with the Vodafone Chair Mobile Communication Systems, Technische Universität Dresden, Germany (e-mail: {ahmad.nimr, gerhard.fettweis}@tu-dresden.de).

Raed M. Shubair is with the Department of Electrical and Computer Engineering, New York University (NYU), Abu Dhabi 129188, UAE (e-mail: rshubair@mit.edu; raed.shubair@nyu.edu).

of each received symbol. After that, super resolution convolutional long short-term memory (SR-ConvLSTM) is employed to improve ADD-TT interpolation accuracy. TS-ChannelNet estimator outperforms the ChannelNet estimator especially in low signal-to-noise ratio (SNR) regions. Moreover, the TS-ChannelNet estimator has lower computational complexity than the ChannelNet estimator since only one CNN network is considered instead of two CNNs as proposed in the ChannelNet estimator.

Nevertheless, TS-ChannelNet also suffers from a considerable performance degradation in high mobility vehicular scenarios. It is worth mentioning that both ChannelNet and TS-ChannelNet estimators suffer from high latency at the receiver, since the receiver should wait for the arrival of the whole frame in order to start the channel estimation process.

In order to overcome the high complexity and performance degradation in high vehicular scenarios, we propose in this paper novel weighted interpolation (WI) channel estimators that employ new pilot allocation schemes for the IEEE 802.11p that insert pilot symbols into the transmitted frame. Unlike ChannelNet and TS-ChannelNet estimators, where the employed interpolation techniques are performed in time and frequency, the developed WI estimators require only weighted time interpolation of the inserted pilot symbols. The number of inserted pilots is controlled by the mobility condition. In particular, one orthogonal frequency-division multiplexing (OFDM) symbol with all pilots is inserted at the end of the transmitted frame in low mobility scenario and as the mobility increases, more pilot OFDM symbols are required. All the other symbols within the transmitted frame are fully allocated by data subcarriers and considered as data symbols. The estimated channel for the data symbols is considered as a weighted summation of the estimated channels at the inserted pilot symbols. According to the employed frame structure, the receiver treats the received frame as subframes, thus achieving lower latency at the receiver, since the channel estimation starts upon receiving each subframe instead of waiting for the whole frame. Moreover, in order to gain more transmission data rate (TDR), few pilots can be inserted within the pilot OFDM symbols depending on the channel delay profile.

On top of that, further performance improvement can be achieved by employing optimized SR-CNN or DN-CNN as post processing modules after the WI estimators. The proposed WI estimators enjoy low-complexity and robustness, and achieve good performance in high-mobility vehicular scenarios. Additionally, employing the proposed WI estimators result in latency reduction at the receiver, besides gaining more transmission data rates. The contributions of this paper can be summarized as follows:

- Proposing a low-complexity, robust WI channel estimators that modify the pilot allocation schemes of the IEEE 802.11p within the transmitted frame.
- Deriving analytically the expression of the employed interpolation matrix for the proposed pilot allocation schemes.
- Providing a brief overview of the CNN networks, especially those employed in the state-of-the-art of the channel estimation, such as SR-CNN, DN-CNN.

- Integrating an optimized SR-CNN and DN-CNN networks on top of the WI estimators to enhance the bit error rate (BER) performance.
- Showing that the proposed WI estimators outperform ChannelNet and TS-ChannelNet estimators in terms of latency and transmission data rates.
- Providing a detailed computational complexity analysis for the studied channel estimators, where we show that the proposed WI estimators outperform the benchmarked estimators with substantial reduction in computational complexity.

The remainder of this paper is organized as follows: in Section II, the IEEE 802.11p standard and the system model are described. Section III provides a detailed description of the recently proposed ChannelNet and TS-ChannelNet estimators. The proposed WI estimators, as well as the analytical interpolation matrices derivations are presented in Section IV. Then, a detailed overview of the CNN based channel estimation and the proposed optimized architectures is provided in Section V. In Section VI, simulation results are presented for different vehicular channel models conditions employing different modulation orders, where the performance of the proposed estimators is evaluated in terms of BER, TDR, and latency. Detailed computational complexity analysis is provided in Section VII. Finally, conclusions are given in Section VIII.

II. SYSTEM MODEL DESCRIPTION

IEEE 802.11p is an international standard that manages wireless access in vehicular environments. IEEE 802.11p defines the communications between high-speed vehicles (vehicle-to-vehicle (V2V)) and between the vehicles and the roadside infrastructure (vehicle-to-infrastructure (V2I)) in the licensed intelligent transportation systems band [16]. IEEE 802.11p employs OFDM transmission scheme with $K = 64$ total subcarriers. $K_{\text{on}} = 52$ active subcarriers are used, and they are divided into $K_{\text{d}} = 48$ data subcarriers and $K_{\text{p}} = 4$ pilot subcarriers. The remaining 12 subcarriers are used as a guard band. IEEE 802.11p standard employs two long training symbols (LTS) preamble symbols at the beginning of the transmitted frame that are used for signal detection and channel estimation at the receiver. Moreover, it supports transmitting data at different data rates employing different modulation orders. Table I shows the IEEE 802.11p physical layer main specifications. A detailed discussion of the IEEE 802.p standard and all its features is presented in [2].

In this paper, we assume perfect synchronization at the receiver, and we consider a frame that consists of two LTS at the beginning followed by I OFDM data symbols. The received OFDM symbol $\tilde{\mathbf{y}}_i[k]$ can be expressed in terms of the transmitted OFDM symbol $\tilde{\mathbf{x}}_i[k]$ as follows

$$\tilde{\mathbf{y}}_i[k] = \tilde{\mathbf{h}}_i[k]\tilde{\mathbf{x}}_i[k] + \tilde{\mathbf{v}}_i[k], \quad k \in \mathcal{K}_{\text{on}}. \quad (1)$$

Here, $\tilde{\mathbf{v}}_i[k]$ denotes the noise of the k -th subcarrier in the i -th OFDM symbol. $\tilde{\mathbf{h}}_i[k]$ represents the time variant frequency response of the channel for the i -th OFDM symbol. Moreover, let $\tilde{\mathbf{Y}}[k, i] \in \mathbb{C}^{K_{\text{on}} \times I}$ and $\tilde{\mathbf{X}}[k, i] \in \mathbb{C}^{K_{\text{on}} \times I}$ be the received and transmitted OFDM frame respectively. Then, (1) can be expressed in a matrix form as follows

Table I: IEEE 802.11p physical layer specifications.

| Parameter | IEEE 802.11p |
|--------------------------------|--------------|
| Bandwidth | 10 MHz |
| Guard interval duration | 1.6 μ s |
| Symbol duration | 8 μ s |
| Short training symbol duration | 1.6 μ s |
| Long training symbol duration | 6.4 μ s |
| Total subcarriers | 64 |
| Pilot subcarriers | 4 |
| Data subcarriers | 48 |
| Null subcarriers | 12 |
| Subcarrier spacing | 156.25 KHz |

$$\tilde{\mathbf{Y}}[k, i] = \tilde{\mathbf{H}}[k, i]\tilde{\mathbf{X}}[k, i] + \tilde{\mathbf{V}}[k, i], \quad k \in \mathcal{K}_{\text{on}}, \quad (2)$$

where $\tilde{\mathbf{V}}[k, i] \in \mathbb{C}^{K_{\text{on}} \times I}$ and $\tilde{\mathbf{H}} \in \mathbb{C}^{K_{\text{on}} \times I}$ denote the noise and the time variant frequency response of the channel for all symbols within the transmitted OFDM frame respectively.

III. SOA OF CNN-BASED CHANNEL ESTIMATORS

In the section, the recently proposed CNN-based estimators schemes are presented and discussed.

A. ChannelNet estimator

In [14], the authors propose a CNN-based channel estimator denoted as ChannelNet scheme, where 2D RBF interpolation is applied as an initial channel estimation, after that the RBF interpolated frame is considered as a low resolution image, where SR-CNN is employed to get better estimation. Finally, in order to alleviate the impact of noise within the high resolution estimated frame, DN-CNN is implemented on top of the SR-CNN resulting in a high resolution, noise alleviated estimated channels. The ChannelNet estimator considers sparsely allocated pilots within the IEEE 802.11p frame and it proceeds as follows:

- LS estimation at pilot subcarriers: the LS estimation at pilot subcarriers is performed as follows:

$$\hat{\mathbf{H}}_{\text{LS}}[k, i] = \frac{\tilde{\mathbf{Y}}[k, i]}{\tilde{\mathbf{P}}[k, i]}, \quad k \in \mathcal{K}_{p_i}, \quad 1 \leq i \leq I. \quad (3)$$

$\hat{\mathbf{H}}_{\text{LS}} \in \mathbb{C}^{K_p \times I}$ denotes the LS estimated channels at the sparsely allocated pilots subcarriers. $\tilde{\mathbf{P}}[k, i]$ is the frequency domain pre-defined pilot subcarriers. \mathcal{K}_{p_i} denotes the allocated sparsely allocated pilots indices within the received OFDM symbol.

- RBF interpolation: the estimated channel at the k -th data subcarrier within the received OFDM frame is obtained by applying the 2D RBF interpolation [17] employing $\hat{\mathbf{H}}_{\text{LS}}$ obtained in (3). The RBF interpolation is obtained by the weighted summation of the distance between each data subcarrier to be interpolated, and all the pilot subcarriers within the received OFDM frame, such that

$$\hat{\mathbf{H}}_{\text{RBF}}[k, i] = \sum_{j=1}^{K_p I} \omega_j \Phi(|k - \mathcal{K}_f[j]|, |i - \mathcal{K}_t[j]|) \quad (4)$$

$\mathcal{K}_f = [\mathcal{K}_{p_1}, \dots, \mathcal{K}_{p_I}] \in \mathbb{R}^{1 \times K_p I}$ and $\mathcal{K}_t = [(1)_{\times K_p}, \dots, (I)_{\times K_p}] \in \mathbb{R}^{1 \times K_p I}$ denote the frequency and time indices vectors of the sparsely allocated pilot subcarriers within the received OFDM frame. ω_j represents the RBF weight multiplied by the RBF interpolation function $\Phi(\cdot)$ between the (k, i) data subcarrier and the $(\mathcal{K}_f[j], \mathcal{K}_t[j])$ pilot subcarrier. In [14], the RBF gaussian function is employed, such that

$$\Phi(x, y) = e^{-\frac{(x+y)^2}{r_0}}, \quad (5)$$

where r_0 is the RBF scale factor and it varies according to the employed RBF function. Moreover, the RBF weights $\mathbf{w}_{\text{RBF}} = [\omega_1, \dots, \omega_{K_p I}] \in \mathbb{R}^{K_p I \times 1}$ are calculated using the following relation

$$\mathbf{A}_{\text{RBF}} \mathbf{w}_{\text{RBF}} = \bar{\mathbf{h}}_{\text{LS}}, \quad (6)$$

where $\bar{\mathbf{h}}_{\text{LS}} = \text{vec} \left\{ \hat{\mathbf{H}}_{\text{LS}} \right\} \in \mathbb{C}^{K_p I \times 1}$, $\mathbf{A}_{\text{RBF}} \in \mathbb{R}^{K_p I \times K_p I}$ is the RBF interpolation matrix of the pilots subcarriers, with entries $a_{i,j} = \Phi(\mathcal{K}_f[i], \mathcal{K}_t[j])$ where $i, j = 1, \dots, K_p I$. After computing \mathbf{w}_{RBF} , the RBF estimated channel for every data subcarriers within the received OFDM frame can be calculated as shown in (4).

- SR-CNN and DN-CNN: the RBF interpolation estimated frame $\hat{\mathbf{H}}_{\text{RBF}}$ is fed as an input to SR-CNN first, in order to improve the channel estimation accuracy. After that, the noise is alleviated by applying DN-CNN to the improved SR-CNN estimated channels.

The ChannelNet estimator suffers from high computational complexity that results from the computation of (6) for the channel estimation of each data subcarrier, besides the high complex SR-CNN and DN-CNN architectures. Moreover, it suffers from considerable performance degradation in low SNR regions and high mobility vehicular scenarios.

B. TS-ChannelNet estimator

TS-ChannelNet [15] has been proposed to tackle the problem of channel estimation in vehicular communications. It is based on applying ADD-TT interpolation to the received OFDM frame. After that, an accurate estimation is obtained by implementing SR-ConvLSTM network in order to track vehicular channel variations by learning the time and frequency correlations of the vehicular channel. First, the LS estimation is applied using the two LTS received preambles denoted as $\tilde{\mathbf{y}}_{\text{LTS}_1}[k]$, and $\tilde{\mathbf{y}}_{\text{LTS}_2}[k]$, and the predefined frequency domain preamble sequence $\tilde{\mathbf{p}}[k]$ such that

$$\hat{\mathbf{h}}_{\text{LTS}}[k] = \frac{\tilde{\mathbf{y}}_{\text{LTS}_1}[k] + \tilde{\mathbf{y}}_{\text{LTS}_2}[k]}{2\tilde{\mathbf{p}}[k]}. \quad (7)$$

After that, decision-directed (DD) channel estimation is applied by employing the demapped data subcarriers of the previous received OFDM symbol to estimate the channel for the current OFDM symbol. The DD estimation consists of the following steps

- 1) Equalization: the i -th received OFDM symbol is equalized by the previously DD estimated channel, such that

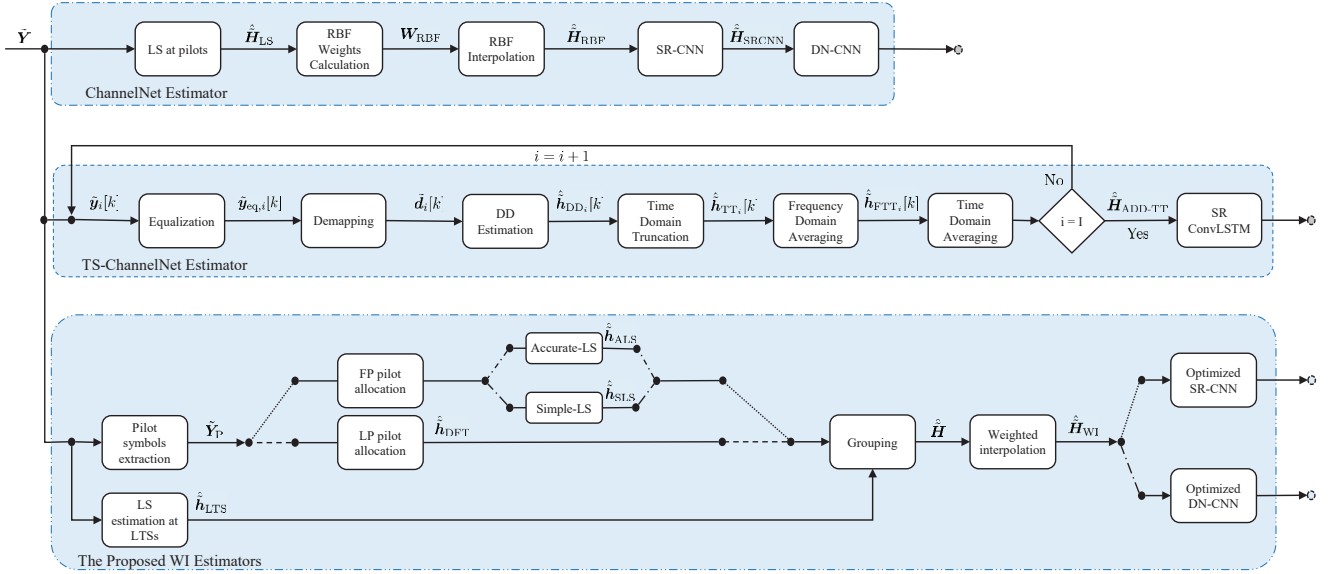


Figure 1: Proposed WI estimators block diagram.

$$\tilde{\mathbf{y}}_{\text{eq}_i}[k] = \frac{\tilde{\mathbf{y}}_i[k]}{\hat{\mathbf{h}}_{\text{ADD-TT}_{i-1}}[k]}, \quad \hat{\mathbf{h}}_{\text{ADD-TT}_0}[k] = \hat{\mathbf{h}}_{\text{LS}}[k]. \quad (8)$$

- 2) Demapping: $\tilde{\mathbf{y}}_{\text{eq}_i}[k]$ is demapped to the nearest constellation point to obtain $\tilde{\mathbf{d}}_i[k]$.
- 3) DD estimation: update the DD estimated channel for the i -th received OFDM symbol, by dividing $\tilde{\mathbf{y}}_i[k]$ with $\tilde{\mathbf{d}}_i[k]$ as expressed below

$$\hat{\mathbf{h}}_{\text{DD}_i}[k] = \frac{\tilde{\mathbf{y}}_i[k]}{\tilde{\mathbf{d}}_i[k]}. \quad (9)$$

It is worth mentioning that the DD estimation suffers from a considerable accumulated demapping error that is enlarged within the frame, especially at low SNR region. Therefore, to reduce its impact, this error $\hat{\mathbf{h}}_{\text{DD}_i}[k]$ is converted to $\hat{\mathbf{h}}_{\text{DD}_i}$ in the time domain using inverse fast Fourier transformation (IFFT), such that

$$\hat{\mathbf{h}}_{\text{DD}_i} = \mathbf{F}_K^H \hat{\mathbf{h}}_{\text{DD}_i}[k], \quad (10)$$

where $\mathbf{F}_K \in \mathbb{C}^{K \times K}$ denotes the K -DFT matrix. Then, by truncating $\hat{\mathbf{h}}_{\text{DD}_i}$ to the significant L channel taps, i.e.

$$\hat{\mathbf{h}}_{\text{DD}_{i,L}} = \hat{\mathbf{h}}_{\text{DD}_i}(1:L). \quad (11)$$

After that, $\hat{\mathbf{h}}_{\text{DD}_{i,L}}$ is converted back to the frequency domain such that

$$\hat{\mathbf{h}}_{\text{TT}_i} = \mathbf{F}_{\text{on}} \hat{\mathbf{h}}_{\text{DD}_{i,L}}, \quad (12)$$

where $\mathbf{F}_{\text{on}} \in \mathbb{C}^{K_{\text{on}} \times L}$ represents the scaled DFT matrix that is used to convert $\hat{\mathbf{h}}_{\text{DD}_{i,L}}$ back to frequency domain, which is obtained by selecting K_{on} rows, and L columns from the K -DFT matrix. Applying the average time truncation operation to $\hat{\mathbf{h}}_{\text{DD}_i}[k]$ alleviates the effect of noise and enlarged demapping error. Moreover, $\hat{\mathbf{h}}_{\text{TT}_i}[k]$ estimated channel is further improved

by applying frequency and time domain averaging consecutively as follows

$$\hat{\mathbf{h}}_{\text{FFT}_i}[k] = \sum_{\lambda=-\beta}^{\lambda=\beta} \omega_{\lambda} \hat{\mathbf{h}}_{\text{TT}_i}[k + \lambda], \quad \omega_{\lambda} = \frac{1}{2\beta + 1}. \quad (13)$$

The final ADD-TT channel estimates is updated using time averaging between the previously ADD-TT estimated channel and the frequency averaged channel in (13), such that

$$\hat{\mathbf{h}}_{\text{ADD-TT}_i}[k] = (1 - \alpha) \hat{\mathbf{h}}_{\text{ADD-TT}_{i-1}}[k] + \alpha \hat{\mathbf{h}}_{\text{FFT}_i}[k]. \quad (14)$$

Motivated by the fact that the vehicular time-variant channel can be modeled as a time-series forecasting problem, where historical data can be used to predict future observations [18]. The authors in [15] apply SR-ConvLSTM network on top of the ADD-TT interpolation, where convolutional layers are added to the LSTM network in order to capture more vehicular channel features, and thus improving the estimation performance. Therefore, the ADD-TT estimated channel for the whole received frame is modeled as a low resolution image, and then SR-ConvLSTM network is employed after the ADD-TT interpolation. Unlike ChannelNet estimator where two CNNs are employed, TS-ChannelNet estimator uses only SR-ConvLSTM network, thus the overall computational complexity is relatively decreased. However, TS-ChannelNet still suffers from high computational complexity due to integrating both LSTM and CNN in one network.

IV. PROPOSED WEIGHTED INTERPOLATION ESTIMATORS

The proposed WI estimators employ different pilot allocation schemes to the IEEE 802.11p frame structure as shown in Fig. 2. The proposed frame structures preserve the first two LTS preamble symbols similar to IEEE 802.11p standard, so that the synchronization and frame detection processes will not be affected by the proposed modifications. Moreover, only P pilot OFDM symbols are required in the transmitted

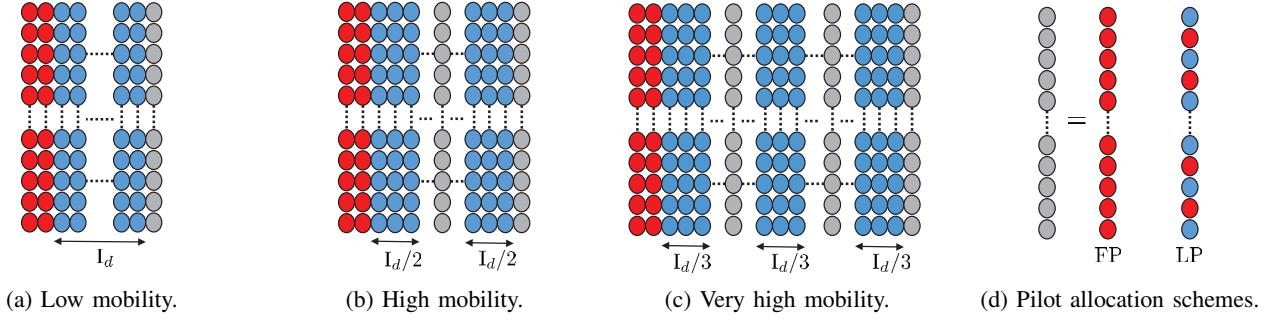


Figure 2: Proposed IEEE 802.11p frame structure employing different pilot allocation schemes.

frame, such that $\tilde{\mathbf{Y}}_P = [\tilde{\mathbf{y}}_1^{(p)}, \dots, \tilde{\mathbf{y}}_q^{(p)}, \dots, \tilde{\mathbf{y}}_P^{(p)}] \in \mathbb{C}^{K_{\text{on}} \times P}$. q denotes the inserted pilot symbol index, where $1 \leq q \leq P$. The other $I_d = I - P$ OFDM data symbols are preserved for actual data transmission.

The proposed estimators proceed according to two criteria: (i) Vehicular mobility condition, where three frame structures are defined as shown in Fig. 2. (ii) The pilot allocation schemes, where there exists two schemes as shown in 2d, such that

- **Full pilot allocation (FP):** where K_{on} pilots are inserted within each pilot symbol and LS estimation is applied to estimate the channel for each inserted pilot symbol. The IEEE 802.11p basic LS denoted as *simple LS (SLS)* estimation is applied using the two LTS received preambles $\tilde{\mathbf{y}}_{\text{LTS}_1}[k]$, and $\tilde{\mathbf{y}}_{\text{LTS}_2}[k]$ as shown in (7), and using each received pilot symbol such that

$$\hat{\mathbf{h}}_{\text{SLS}_q}[k] = \frac{\tilde{\mathbf{y}}_q^{(p)}[k]}{\tilde{\mathbf{p}}[k]} = \tilde{\mathbf{h}}_q[k] + \tilde{\mathbf{v}}_q[k], \quad k \in \mathcal{K}_{\text{on}}. \quad (15)$$

$\tilde{\mathbf{v}}_q[k]$ represents the noise at the q -th received pilot symbol. On the other hand, the *accurate LS (ALS)* relies on the fact that $\tilde{\mathbf{h}}_q = \mathbf{F}_{\text{on}} \mathbf{h}_{q,L}$, where $\mathbf{h}_{q,L} \in \mathbb{C}^{L \times 1}$ denotes the channel impulse response at the q -th received pilot symbol that can be estimated as follows

$$\begin{aligned} \hat{\mathbf{h}}_{q,L} &= \mathbf{F}_{\text{on}}^\dagger \hat{\mathbf{h}}_{\text{LS}_q} \\ &= \mathbf{h}_{q,L} + \mathbf{F}_{\text{on}}^\dagger \tilde{\mathbf{v}}_q, \quad k \in \mathcal{K}_{\text{on}}, \end{aligned} \quad (16)$$

where $\mathbf{F}_{\text{on}}^\dagger = [(\mathbf{F}_{\text{on}}^H \mathbf{F}_{\text{on}})^{-1} \mathbf{F}_{\text{on}}^H]$ is the pseudo inverse matrix of \mathbf{F}_{on} . After that, the accurate LS estimation can be obtained by applying the discrete Fourier transform (DFT) interpolation of $\hat{\mathbf{h}}_{q,L}$ as follows

$$\begin{aligned} \hat{\mathbf{h}}_{\text{ALS}_q} &= \mathbf{F}_{\text{on}} \hat{\mathbf{h}}_{q,L} \\ &= \mathbf{F}_{\text{on}} \mathbf{h}_{q,L} + \mathbf{W}_{\text{ALS}} \tilde{\mathbf{v}}_q, \quad k \in \mathcal{K}_{\text{on}}. \end{aligned} \quad (17)$$

$\mathbf{W}_{\text{ALS}} = \mathbf{F}_{\text{on}} \mathbf{F}_{\text{on}}^\dagger$ denotes the accurate LS DFT interpolation matrix.

- **L pilot allocation (LP):** this allocation is motivated by the fact that vehicular channel models mainly consists of 12 taps, then calculating $\mathbf{h}_{q,L}$ requires only L pilots in each pilot symbol, and can be computed as follows

$$\begin{aligned} \hat{\mathbf{h}}_{q,L} &= \mathbf{F}_p^\dagger \hat{\mathbf{h}}_{\text{LS}_q} \\ &= \mathbf{h}_{q,L} + \mathbf{F}_p^\dagger \tilde{\mathbf{v}}_q, \quad k \in \mathcal{K}_p. \end{aligned} \quad (18)$$

$\hat{\mathbf{h}}_{\text{LS}_q}$ here represents the LS estimated channel for the q -th pilot symbol at the L equally spaced inserted pilot subcarriers, where $K_p = L$ and $\mathbf{F}_p^\dagger = [(\mathbf{F}_p^H \mathbf{F}_p)^{-1} \mathbf{F}_p^H]$ is the pseudo inverse matrix of $\mathbf{F}_p \in \mathbb{C}^{K_p \times L}$ which refers to the truncated DFT matrices obtained by selecting K_p rows, and L columns from the K -DFT matrix. After that, DFT interpolation based estimation can be used employing $\hat{\mathbf{h}}_{q,L}$ to estimate the channel for the q -th pilot symbol as follows

$$\begin{aligned} \hat{\mathbf{h}}_{\text{DFT}_q} &= \mathbf{F}_{\text{on}} \hat{\mathbf{h}}_{q,L} \\ &= \mathbf{F}_{\text{on}} \mathbf{h}_{q,L} + \mathbf{W}_{\text{DFT}} \tilde{\mathbf{v}}_q, \quad k \in \mathcal{K}_{\text{on}}. \end{aligned} \quad (19)$$

Here $\mathbf{W}_{\text{DFT}} = \mathbf{F}_{\text{on}} \mathbf{F}_p^\dagger$ is the DFT interpolation matrix.

After estimating the channel at the pilot symbols according to the selected configuration, the proposed WI estimators apply the following two steps

- **Grouping:** The estimated channels of the P pilot symbols are grouped into P matrices, such that

$$\hat{\mathbf{H}}_q = [\hat{\mathbf{h}}_{q-1}, \hat{\mathbf{h}}_q], \quad q = 1, \dots, P. \quad (21)$$

We note that $\hat{\mathbf{h}}_0 = \hat{\mathbf{h}}_{\text{LTS}}$ and $\hat{\mathbf{h}}_q$ refers to the implemented LS estimation according to the employed pilot allocation scheme.

- **Weighted Interpolation estimation:** According to the grouped $\hat{\mathbf{H}}$ matrices, the received frame can be divided into P sub-frames, where f denotes the sub-frame index, such that $1 \leq f \leq P$. Therefore, the estimated channel for the i -th received OFDM symbol within each f -th sub-frame can be expressed as follows

$$\hat{\mathbf{H}}_{\text{WI}_f} = \hat{\mathbf{H}}_f \mathbf{C}_f \quad (22)$$

where $\hat{\mathbf{H}}_f \in \mathbb{C}^{K_{\text{on}} \times 2}$ denotes LS estimated channels at the pilot symbols within the f -th sub-frame. $\mathbf{C}_f \in \mathbb{R}^{2 \times I_f}$ denotes the interpolation weights of the I_f OFDM data symbols within the f -th sub-frame. We note that I_f is calculated according to the employed frame structure where it is equal to I_d , $\frac{I_d}{2}$, and $\frac{I_d}{3}$ in low, high, and very high mobility scenarios respectively.

Therefore, the estimated channel for the received OFDM data symbols can be seen as a weighted summation of the $\hat{\mathbf{H}}_f$ matrix. \mathbf{C}_f interpolation weights are calculated by minimizing the mean squared error (MSE) between

the ideal channel $\tilde{\mathbf{H}}_f$, and the LS estimated channel at the OFDM pilot symbols $\hat{\tilde{\mathbf{H}}}_f$ as derived in [19]. This minimization results in \mathbf{C}_f expressed in (20), where $J_0(\cdot)$ is the zeroth order Bessel function of the first kind, T_s is the received OFDM data symbol duration, and E_q denotes the overall noise of the estimated channel at the q -th pilot symbol. E_q is calculated according to the chosen pilot allocation scheme, and employed LS estimation, where it equals to σ^2 , $\sigma^2 \text{trace} \{ \mathbf{W}_{\text{ALS}} \mathbf{W}_{\text{ALS}}^H \}$, and $\sigma^2 \text{trace} \{ \mathbf{W}_{\text{DFT}} \mathbf{W}_{\text{DFT}}^H \}$ for SLS, ALS and LP LS estimation respectively.

In fact, the weight elements of \mathbf{C}_f for all the sub-frames can be calculated offline for several vehicular scenarios by employing different f_d and I_d values, Therefore, decreasing the online complexity and making the proposed WI estimators more efficient in real cases scenarios. Moreover, a trade-off between the mobility condition controlled by f_d , the inserted pilot symbols P , and the employed frame length I_d should be considered. As the mobility increases, more pilot symbols should be inserted within the transmitted frame. Therefore, this trade-off is managed by the vehicular application requirements, so that the transmitter will adapt the transmission parameters according to these requirements. Fig. 1 shows the proposed WI estimators block diagram.

V. CNN-BASED CHANNEL ESTIMATION

In this section, a brief description of the CNN and its mathematical model is provided first. After that, the integration of optimized SR-CNN and DN-CNN on top of the proposed WI estimators is described.

A. CNN Overview

A CNN is a neural network that consists of one or more layers and is used mainly for processing structured arrays of data such as images [20]. CNN network has generally become the state of the art for many visual applications such as image classification, due to its great ability in extracting patterns from the input image. CNN is a set of several layers stacked together in order to accomplish the required task. These layers include

- Input layer: It represents the 2D or 3D input image.
- Convolutional layer: It is used for feature extraction that is implemented using predefined filters called kernels. The kernel scans the input matrix to fill the output matrix denoted as feature map.
- Pooling layer: This layer is employed to reduce the number of parameters when the images are too large. Pooling

operation is also called sub-sampling or down-sampling which reduces the dimensionality of each feature map but retains important information.

- Activation layer: An activation function is applied to the CNN layer's output. The most common activation function employed is the ReLU function. It is used to introduce non-linear processing to the CNN architecture since the input-output CNN pairs relation might be non-linear.
- Fully connected layer: This layer forms the last block of the CNN architecture, and it is employed mainly in classification problems. It is a simple feed forward neural network layer, consisting of one or more hidden layers.
- Batch normalization: It is used to make the CNN output more stable by normalizing the output of each layer. Moreover, batch normalisation layer reduces overfitting and speeds up the CNN training.
- Output layer: This layer is configured according to the studied problem, for example, in classification problems the CNN output layer is a fully connected layer with softmax activation function, while in regression problems, the CNN output does not use any activation function.

Automatically detecting meaningful features given only an image and its label is not a trivial task. Therefore, the convolutional layers are the most essential elements within any CNN since the convolutional layers learn such complex features by updating their kernels values during training phase to obtain the best input-output mapping. This update is performed by minimizing the CNN loss function that measures how far are the inputs from the outputs. After that, the performance of the trained CNN model is evaluated in the testing phase where new unobserved inputs are fed to the trained CNN model.

B. SR-CNN and DN-CNN Networks

Besides classifications problems, there are special CNN architectures denoted as SR-CNN and DN-CNN that are mainly used for regression problems. SR-CNN [21] is used to improve the quality of the input image, where the input-output mapping is represented as a deep CNN that takes the low-resolution image as the input and outputs the high-resolution one. SR-CNN consists of three convolutional layers as shown in Fig. 3: (i) Patch extraction and representation, (ii) Non-linear mapping, and (iii) Reconstruction. Let $\mathbf{X}_m \in \mathbb{R}^{h_m \times w_m \times d_m}$ be the input image to the m -th SR-CNN convolutional layer, where h_m , w_m , and d_m denote the image height, width, and depth respectively, and $\mathbf{X}_1 \in \mathbb{R}^{h_1 \times w_1 \times d_1}$ represents the input image. The convolutional filters are denoted by the weights and biases matrices $\mathbf{W}_m \in \mathbb{R}^{v_m \times v_m \times d_m \times f_m}$ and $\mathbf{B}_m \in \mathbb{R}^{f_m \times 1}$, where

$$\begin{aligned} \mathbf{C}_f &= \mathbb{E} \left[\tilde{\mathbf{H}}_f \hat{\tilde{\mathbf{H}}}_f^H \right] \left[\mathbb{E} \left[\hat{\tilde{\mathbf{H}}}_f \hat{\tilde{\mathbf{H}}}_f^H \right] \right]^{-1} = \begin{bmatrix} \mathbb{E} \left[\tilde{\mathbf{H}}_f \hat{\tilde{\mathbf{h}}}_q^H \right] & \mathbb{E} \left[\tilde{\mathbf{H}}_f \hat{\tilde{\mathbf{h}}}_{q+1}^H \right] \\ \mathbb{E} \left[\tilde{\mathbf{h}}_q \tilde{\mathbf{h}}_q^H \right] + E_q & \mathbb{E} \left[\tilde{\mathbf{h}}_q \tilde{\mathbf{h}}_{q+1}^H \right] \\ \mathbb{E} \left[\tilde{\mathbf{h}}_{q+1} \tilde{\mathbf{h}}_q^H \right] & \mathbb{E} \left[\tilde{\mathbf{h}}_{q+1} \tilde{\mathbf{h}}_{q+1}^H \right] + E_{q+1} \end{bmatrix}^{-1} \\ &= \begin{bmatrix} J_0(2\pi f_d(f-1)T_s) & J_0(2\pi f_d(I_f+1-f)T_s) \\ J_0(2\pi f_d I_f T_s) & 1 + E_{q+1} \end{bmatrix} \begin{bmatrix} 1 + E_{\Phi_q} & J_0(2\pi f_d I_f T_s) \\ J_0(2\pi f_d I_f T_s) & 1 + E_{q+1} \end{bmatrix}^{-1}. \end{aligned} \quad (20)$$

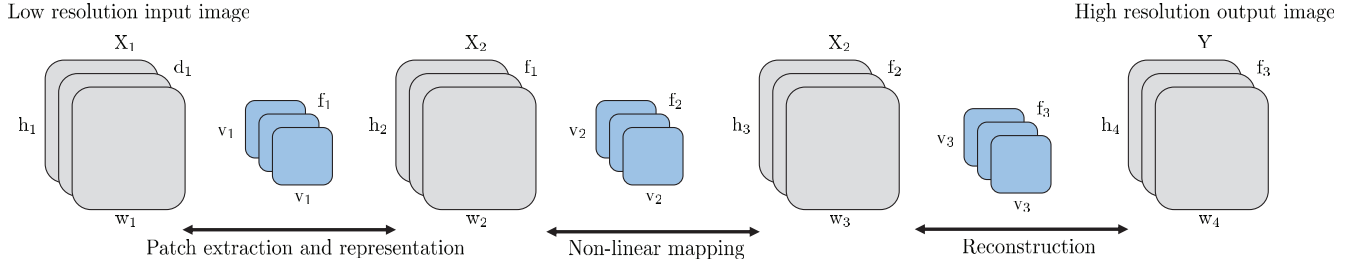


Figure 3: SR-CNN architecture.

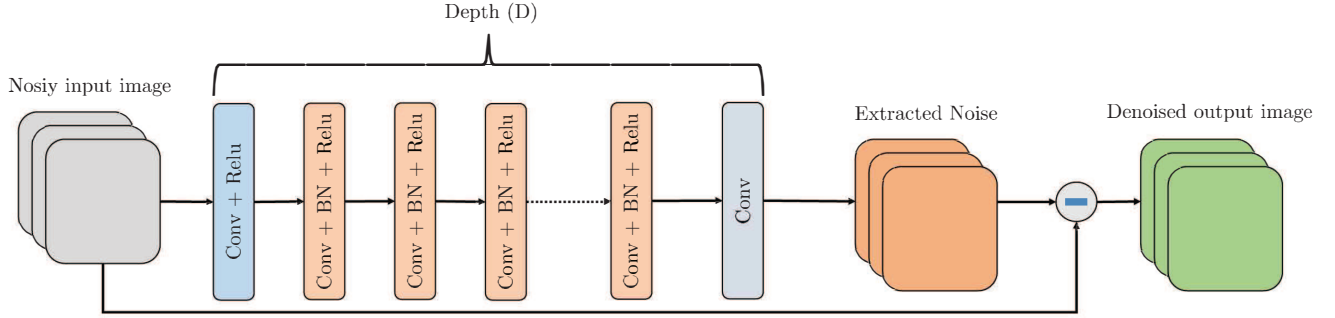


Figure 4: DN-CNN architecture.

v_m refers to the convolutional filter size, and f_m denotes the total number of filters employed in the SR-CNN m -th convolutional layer. The m -th convolution layer applies f_m convolution operation to its X_m input image as follows

$$Y_{(m)} = F_{(m)}\left(W_{(m)} * X_{(m)}\right), X_{(m+1)} = Y_{(m)}, \quad (23)$$

where $F_{(m)}$ represents the activation function applied to the m -th convolutional layer output. We note that, it is possible to add more convolutional layers to increase the non-linearity mapping between the SR-CNN convolutional layers, but this will increase the complexity of the SR-CNN model and thus demands more training time. The employed SR-CNN architecture related mainly to the investigated problem and the dataset structure, whereas the best SR-CNN architecture and parameters can be fine tuned by intensive experiments or by using the grid search algorithm [22] that selects the best suitable SR-CNN hyperparameters in terms of both performance and complexity. The loss function of the SR-CNN is represented by the MSE between the SR-CNN reconstructed high resolution images Y , and the true images $Y^{(T)}$, such that

$$\text{MSE}_{\text{SR-CNN}} = \frac{1}{N_{\text{Train}}} \sum_{i=1}^{N_{\text{Train}}} \left\| Y_i - Y_i^{(T)} \right\|^2, \quad (24)$$

where N_{Train} denotes the number of training samples. The minimization of $\text{MSE}_{\text{SR-CNN}}$ is achieved by updating W and B matrices such that the best input-output mapping is obtained. To do so, various optimizers can be employed such that the stochastic gradient descent [23], root mean square prop [24], and adaptive moment estimation (ADAM) [25].

Table II: Optimized SR-CNN and DN-CNN parameters.

| Parameter | Values |
|--|------------------------------------|
| Input/Output dimensions | $2K_{\text{on}} \times I \times 1$ |
| SRCNN $(v_1, f_1; v_2, f_2; v_3, f_3)$ | (9,32; 1,16; 5,1) |
| DNCNN (v, f) | (3, 16) |
| DNCNN D | 7 |
| Activation function | ReLU |
| Number of epochs | 250 |
| Training samples | 8000 |
| Testing samples | 2000 |
| Batch size | 128 |
| Optimizer | ADAM |
| Loss function | MSE |
| Learning rate | 0.001 |
| Training SNR | 30 dB |

On the other hand, DN-CNN [26] improves the image quality by separating the noise from the input noisy image using a special CNN architecture. After that, the input noisy image is subtracted from the extracted noise resulting in the denoised image. In order to extract the noise from a noisy image, residual learning [27] is employed so that the noise included in the input image is learnt in the DN-CNN training phase by minimizing the following DN-CNN loss function

$$\text{MSE}_{\text{DN-CNN}} = \frac{1}{N_{\text{Train}}} \sum_{i=1}^{N_{\text{Train}}} \left\| V_i - V_i^{(T)} \right\|^2, \quad (25)$$

where V_i represents the extracted noise included in the noisy

Table III: Vehicular channel models characteristics following Jake's Doppler spectrum.

| Channel model | Channel taps | Vehicle velocity [kmph] | Doppler shift [Hz] | Average path gains [dB] | Path delays [ns] |
|---------------|--------------|-------------------------|--------------------|--|--|
| VTV-UC | 12 | 45 | 250 | [0, 0, -10, -10, -10, -17.8, -17.8, -17.8, -21.1, -21.1, -26.3, -26.3] | [0, 1, 100, 101, 102, 200, 201, 202, 300, 301, 400, 401] |
| VTV-SDWW | 12 | 100-200 | 500-1000 | [0, 0, -11.2, -11.2, -19, -21.9, -25.3, -25.3, -24.4, -28, -26.1, -26.1] | [0, 1, 100, 101, 200, 300, 400, 401, 500, 600, 700, 701] |

input image \mathbf{X}_i , and $\mathbf{V}_i^{(T)}$ denotes the exact noise, such that $\mathbf{V}_i^{(T)} = \mathbf{Y}_i^{(N)} - \mathbf{X}_i$. As shown in Fig. 4, the DN-CNN employs in the first layer convolution and ReLU activation function to generate the initial feature maps from the input noisy image. After that, successive (Conv + BN + ReLU) layers are employed to extract the noise features, since the analysis performed in [26] shows that integrating convolution with batch normalization followed by ReLU, can gradually separate the clean image structure from the noisy observation through the DN-CNN hidden layers. Finally, a convolutional layer is used for output image reconstruction. In summary, the DN-CNN architecture has two main tasks: the residual learning is used to learn the noise features, and the batch normalization which is incorporated to speed up training as well as to boost the denoising performance. The main complexity of the DN-CNN architecture lies in its depth (D) that denotes the number of employed (Conv+ BN + ReLU) layers. As D increases the complexity of the DN-CNN architecture increases. Similarly to SR-CNN, all the DN-CNN parameters can be tuned using grid search algorithm.

Unlike ChannelNet estimator, where both SR-CNN and DN-CNN networks are used on top of the RBF interpolation, deep investigations are applied in this paper in order to select the best CNN network configuration that is suitable with the mobility condition. Therefore, an optimized SR-CNN is employed on top of the WI estimators in low mobility scenario, while optimized DN-CNN is employed in high mobility scenario. By doing so, better performance can be achieved with a significant decrease in the overall computational complexity as we will discuss in the next sections. Moreover, our investigations show that by employing the proposed WI estimators, there is no need to use both SR-CNN and DN-CNN, since the computational complexity will be increased without any significant performance gain.

We note that CNNs networks work with real valued data, therefore after applying the WI interpolation estimator, $\hat{\mathbf{H}}_{\text{WI}} \in \mathbb{C}^{K_{\text{on}} \times I_d}$ is converted from complex to real valued domain by stacking the real and imaginary values vertically in one matrix, such that $\hat{\mathbf{H}}_{\text{WI}}^{(R)} \in \mathbb{R}^{2K_{\text{on}} \times I_d}$. Then $\hat{\mathbf{H}}_{\text{WI}}^{(R)}$ is fed as an input to the optimized SR-CNN or DN-CNN according to the mobility scenario. Finally, the output of the employed network is converted back to the complex domain. The optimized SR-CNN and DN-CNN networks are trained on SNR= 30 dB for each mobility scenario, since in high SNR region, the CNN network is able to learn better the channel due to the low noise impact in high SNR region [28]. Moreover, ADAM optimizer is used with MSE loss function. Table II shows the proposed optimized SR-CNN and DN-CNN parameters.

VI. SIMULATION RESULTS

In this section, the performance of the proposed WI estimators is evaluated compared to ChannelNet and TS-ChannelNet estimators using BER. The simulations are conducted employing QPSK and 16QAM modulation orders with OFDM frame length $I = 100$ in three vehicular scenarios as shown in Table III. These scenarios are based on the tapped delay line (TDL) vehicular channel models proposed in [29], which are obtained by a measurement campaign that was implemented in metropolitan Atlanta, and can be defined as follows

- **Low mobility:** where VTV Urban Canyon (VTV-UC) vehicular channel model is employed. VTV-UC channel model has been measured between two vehicles moving in a dense urban traffic environment at $V = 45$ Kmph which is equivalent to $f_d = 250$ Hz.
- **High mobility:** This scenario measures the communication channel between two vehicles moving on a highway having center wall between its lanes. Moreover, the vehicles are moving in the same direction at $V = 100$ Kmph which is equivalent to $f_d = 500$ Hz with a 300–400 m separation distance between them. This vehicular channel model is denoted as VTV Expressway Same Direction with Wall (VTV-SDWW).
- **Very high mobility:** In order to further evaluate the performance of the benchmarked channel estimators, VTV-SDWW vehicular channel model is employed with $V = 200$ Kmph which implies $f_d = 1000$.

Fig. 5, Fig. 6, and Fig. 7 depict the BER performance employing QPSK and 16QAM modulation of low mobility, high mobility, and very high mobility vehicular scenarios respectively. In low mobility vehicular scenario, the proposed WI-LP estimator records almost similar performance as the TS-ChannelNet estimator, while the proposed WI-FP-SLS estimator slightly outperform the proposed WI-LP estimator by around 1 dB gain in terms of SNR for a BER = 10^{-3} . On the other hand, the performance superiority of the proposed WI-FP-ALS estimator is clearly shown especially in low SNR region, where it outperforms ChannelNet and TS-ChannelNet estimators by around 6 dB and 3 dB gain in terms of SNR for a BER = 10^{-3} , respectively. Moreover, our intensive experiments show that in low mobility scenarios, employing the optimized SR-CNN on top of the proposed WI estimators improves their performance by 1 dB gain in terms of SNR for a BER = 10^{-3} .

For high mobility vehicular scenario, it can be noticed from Fig 6b that the proposed WI-LP suffers from performance degradation especially when 16QAM modulation is employed.

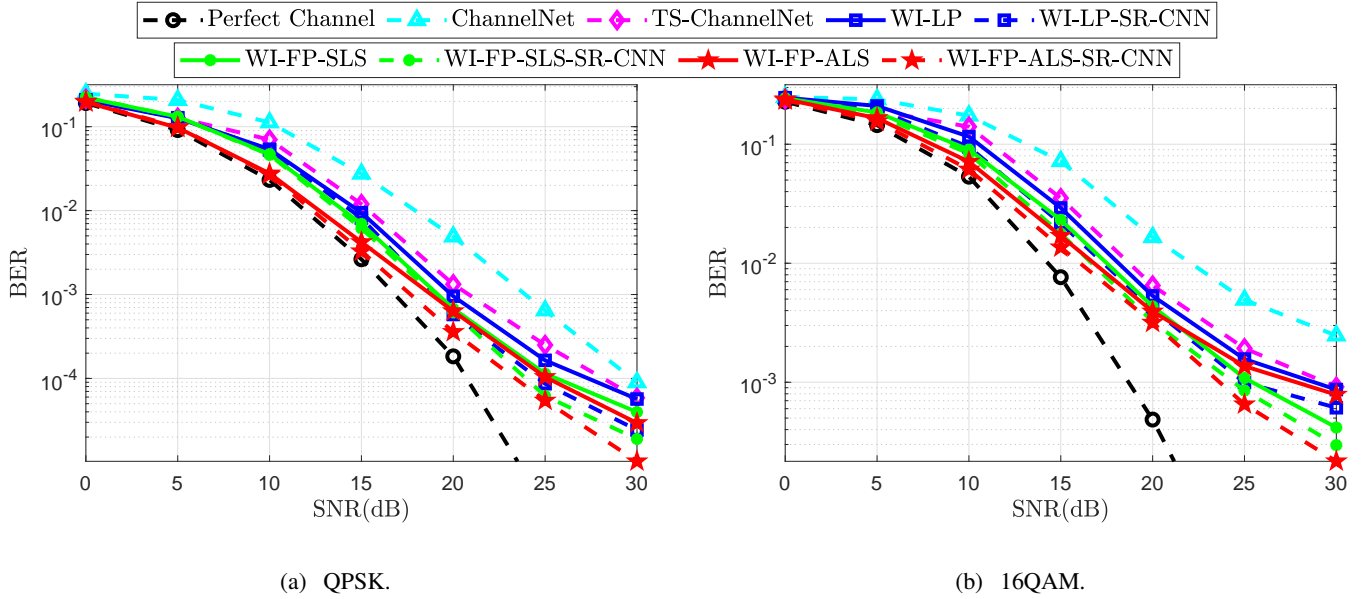


Figure 5: VTV-UC low mobility vehicular channel model BER simulation results.

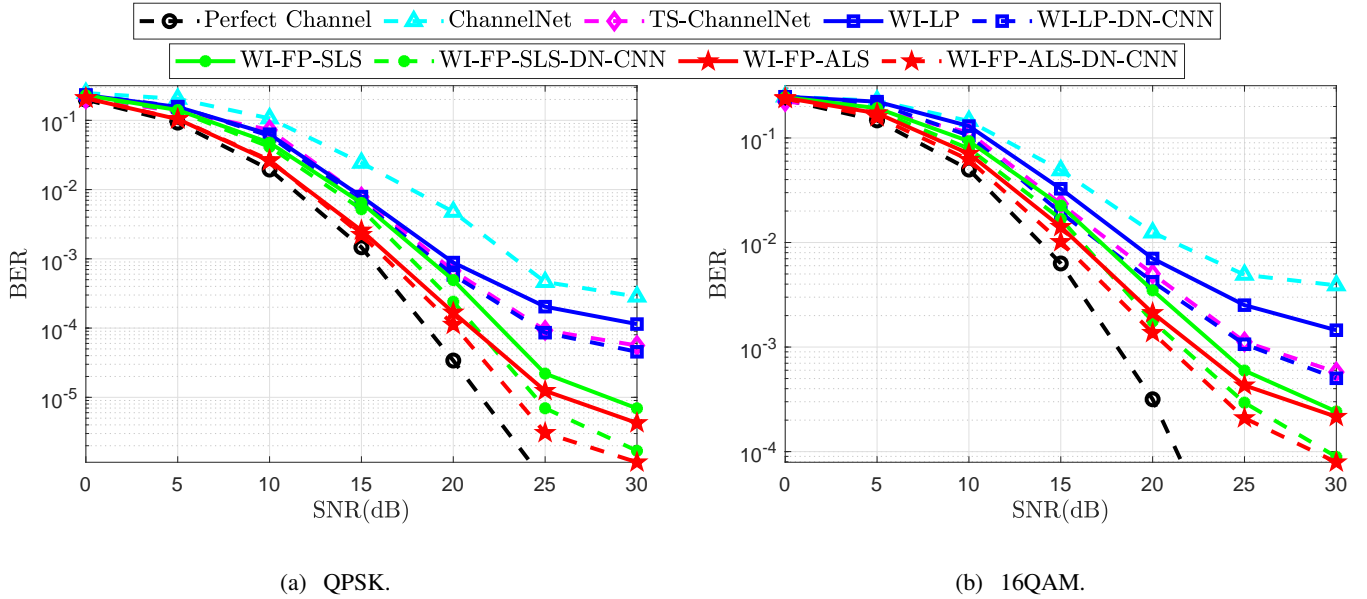


Figure 6: VTV-SDWW high mobility vehicular channel model BER simulation results.

Moreover, employing the optimized DN-CNN on top of the proposed estimators improves the performance, especially in high SNR region, where WI-FP-ALS-DN-CNN outperforms the ChannelNet and TS-ChannelNet estimators by around 8 dB and 4 dB gain in terms of SNR for a $\text{BER} = 10^{-3}$ respectively, while WI-LP-DN-CNN records almost similar performance as the TS-ChannelNet estimator.

In very high mobility scenario Fig 7, the proposed WI-FP-SLS estimator achieves almost similar performance as the TS-ChannelNet estimator, while it outperforms the ChannelNet estimator by around 3 dB gain in terms of SNR for a $\text{BER} = 10^{-3}$. Moreover, at least 4 dB gain can be achieved by employing the optimized DN-CNN on top of the proposed WI-FP-SLS and WI-FP-ALS estimators when QPSK modulation

is employed, while WI-FP-ALS-DN-CNN records a significant performance superiority compared with the other estimators in the whole SNR region, when 16QAM modulation is employed.

It is clearly shown from the simulation results that the TS-ChannelNet estimator is better than the ChannelNet estimator due to the ability of the SR-ConvLSTM network in tracking the vehicular channel variations over time, especially in high mobility scenarios. However, employing the proposed WI estimators, specifically the WI-FP-ALS estimator, significantly outperforms the TS-ChannelNet estimator. This is due to the fact that, the WI is based on employing the past and the future estimated channels at the inserted OFDM pilot symbols, unlike the ADD-TT interpolation where the channel estimation is performed for each received OFDM symbol separately.

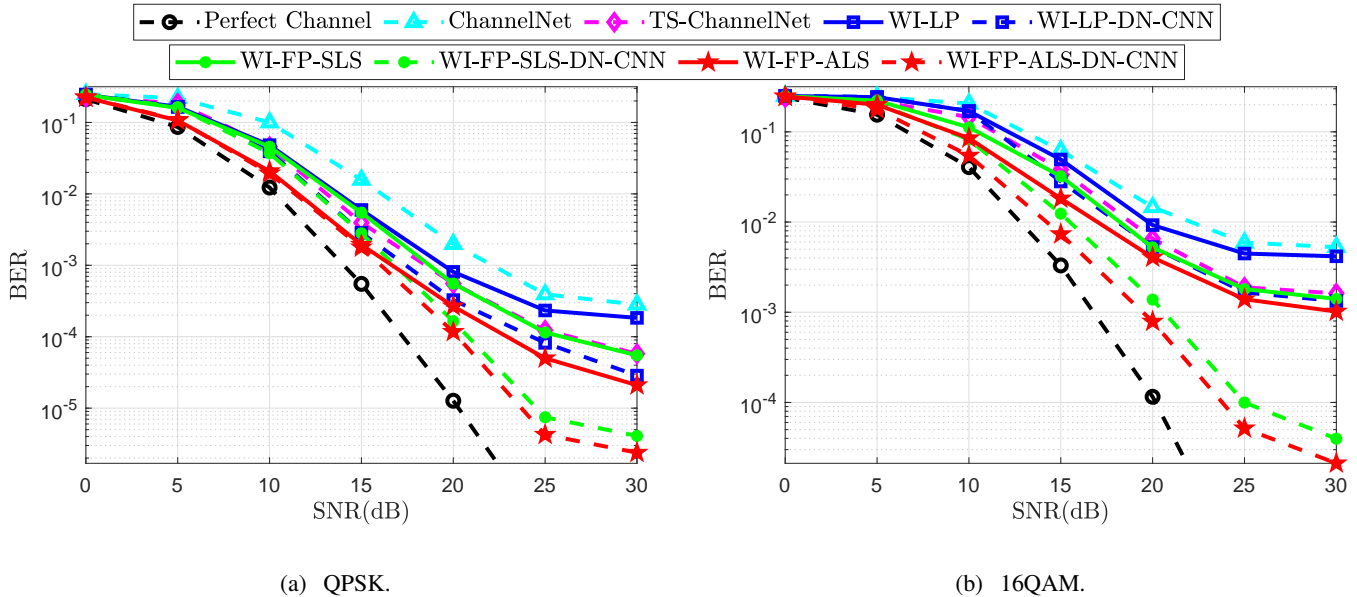


Figure 7: VTV-SDWW very high mobility vehicular channel model BER simulation results.

Moreover, our simulations show that as the accuracy of the employed interpolation technique increases, less complex CNN architectures are required. Therefore, the key points in the proposed WI estimators performance superiority are in the robustness of the employed WI, and the low complex CNN architectures employed that leads to a significant decrease in the overall computational complexity as we discuss in the next section.

It is worth mentioning that employing the optimized SR-CNN on top of the proposed WI estimators in high and very high mobility scenarios leads to a slight performance improvement, while employing the optimized DN-CNN leads to a considerable improvement due to the dominant impact of noise in such scenarios. We note that employing the optimized DN-CNN on top of the optimized SR-CNN will have no worthwhile BER performance gain in all the considered vehicular scenarios. This can be justified by the good performance of the proposed WI estimators before employing any CNN network. However, in order to achieve better performance with acceptable computational complexity increase, the optimized SR-CNN can be employed in low mobility scenario, while the optimized DN-CNN is more useful in high and very high mobility scenarios.

VII. COMPUTATIONAL COMPLEXITY ANALYSIS

In this section, a detailed computational complexity, TDR, and latency analysis of the ChannelNet, TS-ChannelNet, and the proposed WI estimators are presented.

A. Computational Complexity Analysis

The computational complexity is expressed in terms of real valued multiplication/division and summation/subtraction mathematical operations required for a full OFDM frame channel estimation. Each complex-valued division requires 6 real valued multiplications, 2 real valued divisions, 2 real

valued summations, and 1 real valued subtraction. On the other hand, each complex valued multiplication can be expressed by 4 real valued multiplications, and 3 real valued summations.

1) *ChannelNet estimator*: The ChannelNet estimator employs the RBF interpolation followed by SR-CNN and DN-CNN networks. Thus, the overall computational complexity of the ChannelNet estimator can be expressed as follows

$$CC_{\text{ChannelNet}} = CC_{\text{RBF}} + CC_{\text{SR-CNN}} + CC_{\text{DN-CNN}}. \quad (26)$$

As shown in (3), the calculation of $\hat{\mathbf{H}}_{\text{LS}}$ requires $2K_p I$ divisions. \mathbf{w}_{RBF} calculation requires $4K_p^2 I^2$ multiplications/divisions and $5K_p^2 I^2 - 2K_p I$ summations/subtractions. On the other hand, $\hat{\mathbf{H}}_{\text{RBF}}$ computation requires $K_d I(K_p^2 I^2 + 3K_p I)$ multiplications/divisions and $5K_d K_p I^2$ subtractions/summations. Therefore the total computational complexity of the RBF interpolation can be expressed by $K_p^2 I^2(4 + K_d I) + K_p I(2 + 3K_d I)$ multiplications/divisions and $K_p I(5K_p I + 5K_d I - 2)$ summations/subtractions.

After that, The ChannelNet estimator applies SR-CNN followed by DN-CNN on top of the RBF interpolation. The employed SR-CNN consists of three convolutional layers with $(v_1 = 9; f_1 = 64)$, $(v_2 = 1, f_2 = 32)$ and $(v_3 = 5, f_3 = 1)$ respectively. Moreover, DN-CNN depth is $D = 18$ with $3 \times 3 \times 32$ kernels in each layer. $CC_{\text{SR-CNN}}$ and $CC_{\text{DN-CNN}}$ can be computed as follows

$$\begin{aligned} CC_{\text{SR-CNN}} &= \sum_{j=1}^J h_j w_j d_j v_j^2 f_j + h_j w_j d_j f_j \\ &= \sum_{j=1}^J h_j w_j d_j f_j (v_j^2 + 1). \end{aligned} \quad (27)$$

$$CC_{\text{DN-CNN}} = \sum_{j=1}^J h_j w_j d_j f_j (v_j^2 + 1) + \sum_{j=1}^D 4h_j w_j d_j, \quad (28)$$

Table IV: Overall computation complexity in terms of the total required real valued operations.

| Scheme | Interpolation | | CNN | |
|---------------|--|-------------------------------|------------------|-----------------|
| | Mul./Div. | Sum./Sub. | Mul./Div. | Sum./Sub. |
| ChannelNet | $K_p^2 I^2 (4 + K_d I) + K_p I (2 + 3K_d I)$ | $K_p I (5K_p I + 5K_d I - 2)$ | $350144K_{on}I$ | $42432K_{on}I$ |
| TS-ChannelNet | $24K_{on}I + 4LK_{on}I$ | $18K_{on}I + 5K_{on}IL$ | $226880K_{on}I$ | $81472K_{on}I$ |
| FP-SLS-SR-CNN | $2K_{on}P + 2K_{on} + 4K_{on}I_d$ | $2K_{on} + 2K_{on}I_d$ | $7008K_{on}I_d$ | $1120K_{on}I_d$ |
| FP-ALS-SR-CNN | $4K_{on}^2P + 2K_{on}P + 2K_{on} + 4K_{on}I_d$ | $5K_{on}^2P + 2K_{on}I_d$ | | |
| LP-SR-CNN | $2LP + 4K_{on}LP + 2K_{on} + 4K_{on}I_d$ | $5K_{on}LP + 2K_{on}I_d$ | | |
| FP-SLS-DN-CNN | $2K_{on}P + 2K_{on} + 4K_{on}I_d$ | $2K_{on} + 2K_{on}I_d$ | $84096K_{on}I_d$ | $9856K_{on}I_d$ |
| FP-ALS-DN-CNN | $4K_{on}^2P + 2K_{on}P + 2K_{on} + 4K_{on}I_d$ | $5K_{on}^2P + 2K_{on}I_d$ | | |
| LP-DN-CNN | $2LP + 4K_{on}LP + 2K_{on} + 4K_{on}I_d$ | $5K_{on}LP + 2K_{on}I_d$ | | |

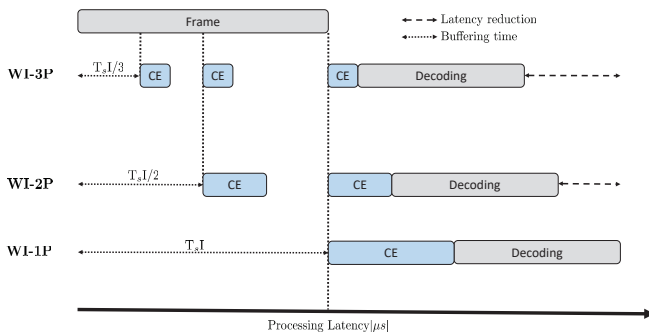


Figure 8: Processing latency of the proposed WI estimators.

where J denotes the number of employed CNN layers. We note that the second term in CC_{DN-CNN} represents the number of operations required by the batch normalization employed in the DN-CNN network. Therefore, the SR-CNN employed in the ChannelNet estimator requires $16064K_{on}I$ multiplications/divisions and $4288K_{on}I$ summations/subtractions, while the ChannelNet DN-CNN computations require $334080K_{on}I$ multiplications/divisions and $38144K_{on}I$ summations/subtractions.

2) *TS-ChannelNet estimator*: The TS-ChannelNet estimator applies the ADD-TT interpolation followed by the SR-ConvLSTM network. Thus, the overall computational complexity of the TS-ChannelNet estimator can be expressed as follows

$$CC_{TS-ChannelNet} = CC_{ADD-TT} + CC_{SR-ConvLSTM}. \quad (29)$$

The employed ADD-TT interpolation The ADD-TT interpolation applies two equalization steps (8), and (9) after the LS estimation in (7) that requires $2K_{on}$ summations, and $2K_{on}$ divisions. Each equalization step consists of K_{on} complex valued division, therefore the equalization in (8), and (9) requires $16K_{on}$ multiplications/divisions and $6K_{on}$ summations/subtractions. The time domain truncation operation applied in (12) requires $4LK_{on}$ multiplications and $5K_{on}L - 2K_{on}$ summations. After time domain truncation, the ADD-TT interpolation applies frequency and time domain averaging. The frequency domain averaging (13) requires $10K_{on}$ summations, and $2K_{on}$ multiplications. Moreover, the time domain averaging step (14), requires $4K_{on}$ real valued divisions, and $2K_{on}$ real valued summations. Therefore, the overall

computational complexity of the ADD-TT interpolation for the whole received OFDM frame requires $24K_{on}I + 4LK_{on}I$ real valued multiplications/divisions, and $18K_{on}I + 5K_{on}IL$ real valued summations/subtractions. On the other hand, the SR-ConvLSTM network consists of three ConvLSTM layers of $(v_1 = 9; f_1 = 64)$, $(v_2 = 1, f_2 = 32)$ and $(v_3 = 5, f_3 = 1)$ respectively. We note that, the SR-ConvLSTM network combines both the CNN and the long short-term memory (LSTM) networks [30], and its computational complexity is expressed in terms of the overall operations applied in the input, forget, and output gates of the SR-ConvLSTM network, such that

$$CC_{ConvLSTM} = \sum_{j=1}^J h_j w_j d_j f_j (8v_j^2 + 30). \quad (30)$$

Based on (30), the SR-ConvLSTM network employed in the TS-ChannelNet estimator requires $226880K_{on}I$ multiplications/divisions and $81472K_{on}I$ summations/subtractions.

TS-ChannelNet estimator is less complex than the ChannelNet estimator, since it employs only one CNN on top of the ADD-TT interpolation, unlike the ChannelNet estimator where both SR-CNN and DN-CNN are employed.

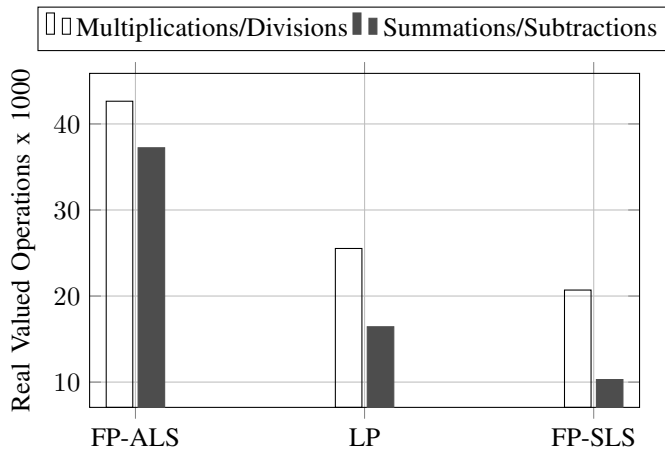
3) *Proposed WI estimators*: The proposed WI estimators computational complexity depend mainly on the selected frame structure, the pilot allocation scheme, and the selected optimized CNN. The overall computational complexity of the proposed WI estimators can be expressed as follows

$$CC_{WI} = CC_{\hat{H}_{WI}} + CC_{O-CNN}. \quad (31)$$

In the case of inserting full pilot symbols, there are two options, the SLS estimator where it requires only $2K_{on}P + 2K_{on}$ divisions, and $2K_{on}$ summations. The second option is employing the ALS estimator, where $2K_{on}P + 2K_{on}$ divisions, followed by $4K_{on}^2P$ multiplications, and $5K_{on}^2P$ summations are required. On the other hand, when $K_p = L$ pilots are inserted with each pilot symbol, then the LS estimation requires $2LP + 2K_{on}$ divisions, $4K_{on}LP$ multiplications, and $5K_{on}LP$ summations. After selecting the required frame structure and pilot allocation scheme, the proposed estimators apply the weighted interpolation as shown in (22), where the channel estimation for each received OFDM frame requires $4K_{on}I_d$ divisions and $2K_{on}I_d$ summations. Finally, the optimized SR-CNN is employed in low mobility scenario and it requires $7008K_{on}I_d$ multiplications/divisions and $1120K_{on}I_d$ summations/subtractions, while the optimized DN-CNN employed in high and very high mobility scenarios requires

Table V: Transmission data rate and buffering time analysis for the benchmarked schemes.

| Scheme | ChannelNet | TS-ChannelNet | Proposed 2D WI | | | | | |
|----------------------|------------|---------------|----------------|-------|-------|-------|-------|-------|
| | | | WI-1P | | WI-2P | | WI-3P | |
| | | | FP | LP | FP | LP | FP | LP |
| TDR gain | 0 % | 0% | 7.25% | 8.08% | 6.16% | 7.83% | 5.08% | 7.58% |
| φ [μ s] | 800 | 800 | 800 | | 400 | | 265 | |

Figure 9: Computational complexities of the proposed WI estimators employing $P = 2$.

$84096K_{on}I_d$ multiplications/divisions and $9856K_{on}I_d$ summations/subtractions

The proposed WI-FP-ALS records the higher computational complexity among the other proposed estimators in all mobility scenarios, due to the \mathbf{W}_{ALS} calculation in (17). Moreover, the proposed WI-FP-SLS estimator is the simplest one. Fig. 9 shows the computational complexity of the proposed WI estimators employing $P = 2$ pilot symbols within the transmitted frame.

Table IV shows the overall computational complexity of the benchmarked estimators in terms of real valued operations. It is worth mentioning that the proposed WI estimators achieve a significant computational complexities decrease compared to ChannelNet and TS-ChannelNet estimators. Fig. 10 shows the compared to the FP-ALS-SR-CNN estimator. The ChannelNet and TS-ChannelNet estimators are 70 and 39 times more complex than the proposed FP-ALS-SR-CNN estimator respectively. We note that FP-ALS-DN-CNN is 12 times more complex than FP-ALS-SR-CNN since the optimized DN-CNN architecture complexity that is employed in high and very high scenarios is higher than the optimized SR-CNN architecture which is used in low mobility scenario.

B. Transmission data rate and latency analysis

The TDR and the latency introduced at the receiver in order to recover the transmitted bits are important issues in vehicular communications, especially when real time applications are employed [31]. The transmission data rate is influenced by

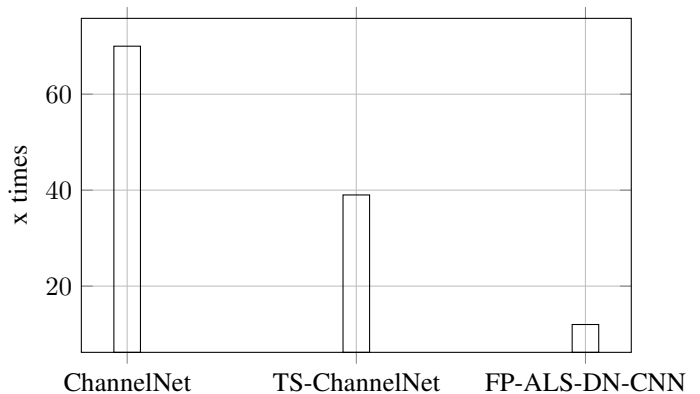


Figure 10: Computational complexities of the benchmarked estimators compared to FP-ALS-SR-CNN.

the number of allocated data subcarriers within the transmitted frame, such that

$$\text{TDR} = \frac{K_{DF} \log_2(M)\rho}{T_s I}, \quad (32)$$

where K_{DF} and ρ denote the total allocated data subcarriers within the transmitted frame, and the employed code rate respectively, and M represents the employed modulation order. Moreover, the buffering time φ can be expressed by the total duration that the receiver should wait before starting the channel estimation, such that

$$\varphi = T_s I. \quad (33)$$

where T_s represents the received OFDM data symbol duration. ChannelNet and TS-ChannelNet estimators employ $K_p = 4$ pilot subcarriers within each transmitted OFDM symbol, however ChannelNet estimator requires sparse pilot allocation within the transmitted OFDM frame, thus increasing the complexity of pilots extraction at the receiver, since the allocated pilots subcarriers indices differs between the OFDM symbols within the frame. Therefore, ChannelNet and TS-ChannelNet estimators have similar transmission data rate as defined in the IEEE 802.11p standard. On the other hand, ChannelNet and TS-ChannelNet estimators suffer from high buffering time at the receiver, since the full frame should be received before the channel estimation starts, thus leading to high latency.

As shown in Table V, the proposed WI estimators record different TDRs gains according to the employed frame structure. Moreover, the proposed WI-2P and WI-3P estimators require lower buffering time than the proposed WI-1P, ChannelNet, and TS-ChannelNet estimators, since it divides the frame into several sub frames as shown in Fig. 8. Thus, the

channel estimation process starts earlier. Therefore, the proposed WI estimators contribute in reducing the total required latency. Finally, we note that the transmission parameters and the chosen frame structure should be adapted according to the mobility condition, required data rate, and the acceptable latency by the vehicular application.

VIII. CONCLUSION

In this paper, channel estimation in vehicular communication is studied. The recently proposed CNN-based channel estimators have been extensively surveyed. Moreover, we have proposed robust WI channel estimators for the IEEE 802.11p standard, where pilot symbols are inserted within the transmitted frame, with several pilot allocation schemes adapted according to the mobility condition. Unlike the recently proposed ChannelNet and TS-ChannelNet estimators that suffer from high computational complexity, performance degradation in high mobility vehicular scenarios, and high latency at the receiver, the proposed WI estimators have reduced computational complexity and robustness in high mobility scenarios. Moreover, they require low buffering time at the receiver and more TDR gain is achieved since all the OFDM symbols within the transmitted frame are fully allocated to data. Additionally, the employed SR-CNN and DN-CNN architectures are optimized through intensive experiments in order to alleviate the high complexity problem. Simulation results have shown the performance superiority of the proposed WI estimators over ChannelNet and TS-ChannelNet estimators in all vehicular scenarios with a substantial reduction in computational complexity, where the ChannelNet and the TS-ChannelNet estimators are more complex than the proposed WI-FP-ALS-SR-CNN by 70 and 39 times respectively.

REFERENCES

- [1] C. F. Mecklenbrauker, A. F. Molisch, J. Karedal, F. Tufvesson, A. Paier, L. Bernado, T. Zemen, O. Klemp, and N. Czink, "Vehicular channel characterization and its implications for wireless system design and performance," *Proceedings of the IEEE*, vol. 99, no. 7, pp. 1189–1212, 2011.
- [2] A. Abdelgader and L. Wu, "The physical layer of the IEEE 802.11 p wave communication standard: The specifications and challenges," vol. 2, 10 2014.
- [3] J. A. Fernandez, K. Borries, L. Cheng, B. V. K. Vijaya Kumar, D. D. Stencil, and F. Bai, "Performance of the 802.11p Physical Layer in Vehicle-to-Vehicle Environments," *IEEE Transactions on Vehicular Technology*, vol. 61, no. 1, pp. 3–14, 2012.
- [4] Z. Zhao, X. Cheng, M. Wen, B. Jiao, and C. Wang, "Channel Estimation Schemes for IEEE 802.11p Standard," *IEEE Intelligent Transportation Systems Magazine*, vol. 5, no. 4, pp. 38–49, 2013.
- [5] Yoon-Kyeong Kim, Jang-Mi Oh, Yoo-Ho Shin, and Cheol Mun, "Time and frequency domain channel estimation scheme for IEEE 802.11p," in *17th International IEEE Conference on Intelligent Transportation Systems (ITSC)*, 2014, pp. 1085–1090.
- [6] T. Wang, C.-K. Wen, H. Wang, F. Gao, T. Jiang, and S. Jin, "Deep learning for wireless physical layer: Opportunities and challenges," 2017.
- [7] T. O'Shea and J. Hoydis, "An introduction to deep learning for the physical layer," *IEEE Transactions on Cognitive Communications and Networking*, vol. 3, no. 4, pp. 563–575, 2017.
- [8] Y. Yang, F. Gao, X. Ma, and S. Zhang, "Deep learning-based channel estimation for doubly selective fading channels," *IEEE Access*, vol. 7, pp. 36 579–36 589, 2019.
- [9] X. Ma, H. Ye, and Y. Li, "Learning assisted estimation for time-varying channels," in *2018 15th International Symposium on Wireless Communication Systems (ISWCS)*, 2018, pp. 1–5.
- [10] H. Ye, G. Y. Li, and B. Juang, "Power of deep learning for channel estimation and signal detection in ofdm systems," *IEEE Wireless Communications Letters*, vol. 7, no. 1, pp. 114–117, 2018.
- [11] S. Han, Y. Oh, and C. Song, "A Deep Learning Based Channel Estimation Scheme for IEEE 802.11p Systems," in *IEEE International Conference on Communications (ICC)*, 2019, pp. 1–6.
- [12] A. K. Gizzini, M. Chafii, A. Nimr, and G. Fettweis, "Deep learning based channel estimation schemes for IEEE 802.11p standard," *IEEE Access*, vol. 8, pp. 113 751–113 765, 2020.
- [13] A. K. Gizzini, M. Chafii, A. Nimr, and G. Fettweis, "Joint TRFI and Deep Learning for Vehicular Channel Estimation," in *IEEE GLOBECOM 2020*, Taipei, Taiwan, Dec. 2020. [Online]. Available: <https://hal.archives-ouvertes.fr/hal-02951636>
- [14] M. Soltani, V. Pourahmadi, A. Mirzaei, and H. Sheikhzadeh, "Deep learning-based channel estimation," *IEEE Communications Letters*, vol. 23, no. 4, pp. 652–655, 2019.
- [15] X. Zhu, Z. Sheng, Y. Fang, and D. Guo, "A deep learning-aided temporal spectral channelnet for IEEE 802.11p-based channel estimation in vehicular communications," *EURASIP Journal on Wireless Communications and Networking*, vol. 1, no. 94, 2020.
- [16] X. Weidong, G. Javier, N. Zhisheng, A. Onur, and E. Eylem, "Wireless Access in Vehicular Environments," *EURASIP Journal on Wireless Communications and Networking*, vol. 1, pp. 1687–1499, 2009.
- [17] W. Toit, "Radial basis function interpolation," *Master Thesis dissertation, Department of Mathematical Sciences University of Stellenbosch, Matieland, South Africa*, 2008.
- [18] C. Chatfield, *Time-Series Forecasting*. Chapman and Hall/CRC, 2000.
- [19] Y. R. Zheng and C. Xiao, "Channel Estimation for Frequency-Domain Equalization of Single-Carrier Broadband Wireless Communications," *IEEE Transactions on Vehicular Technology*, vol. 58, no. 2, pp. 815–823, 2009.
- [20] S. Albawi, T. A. Mohammed, and S. Al-Zawi, "Understanding of a convolutional neural network," in *2017 International Conference on Engineering and Technology (ICET)*, 2017, pp. 1–6.
- [21] C. Dong, C. C. Loy, K. He, and X. Tang, "Image super-resolution using deep convolutional networks," *IEEE Transactions on Pattern Analysis and Machine Intelligence*, vol. 38, no. 2, pp. 295–307, 2016.
- [22] F. Pontes, G. Amorim, P. Balestrassi, A. Paiva, and J. Ferreira, "Design of experiments and focused grid search for neural network parameter optimization," *Neurocomputing*, vol. 186, pp. 22 – 34, 2016.
- [23] J. Schmidhuber, "Deep learning in neural networks: An overview," *Neural Networks*, vol. 61, p. 85–117, Jan 2015. [Online]. Available: <http://dx.doi.org/10.1016/j.neunet.2014.09.003>
- [24] S. ichi Amari, "Backpropagation and stochastic gradient descent method," *Neurocomputing*, vol. 5, no. 4, pp. 185 – 196, 1993. [Online]. Available: <http://www.sciencedirect.com/science/article/pii/0925231293900060>
- [25] S. De, A. Mukherjee, and E. Ullah, "Convergence guarantees for rmsprop and adam in non-convex optimization and an empirical comparison to nesterov acceleration," 2018.
- [26] K. Zhang, W. Zuo, Y. Chen, D. Meng, and L. Zhang, "Beyond a gaussian denoiser: Residual learning of deep CNN for image denoising," *IEEE Transactions on Image Processing*, vol. 26, no. 7, pp. 3142–3155, 2017.
- [27] K. He, X. Zhang, S. Ren, and J. Sun, "Deep residual learning for image recognition," 2015.
- [28] A. K. Gizzini, M. Chafii, A. Nimr, and G. Fettweis, "Enhancing least square channel estimation using deep learning," in *2020 IEEE 91st Vehicular Technology Conference (VTC2020-Spring)*, 2020, pp. 1–5.
- [29] G. Acosta-Marum and M. A. Ingram, "Six time- and frequency- selective empirical channel models for vehicular wireless lans," *IEEE Vehicular Technology Magazine*, vol. 2, no. 4, pp. 4–11, 2007.
- [30] X. Shi, Z. Chen, H. Wang, D.-Y. Yeung, W. Kin Wong, and W. Chun Woo, "Convolutional lstm network: A machine learning approach for precipitation nowcasting," 2015.
- [31] M. I. Ashraf, Chen-Feng Liu, M. Bennis, and W. Saad, "Towards low-latency and ultra-reliable vehicle-to-vehicle communication," in *2017 European Conference on Networks and Communications (EuCNC)*, 2017, pp. 1–5.